International Journal of Heat and Mass Transfer 121 (2018) 759–774

Contents lists available at ScienceDirect

International Journal of Heat and Mass Transfer

journal homepage: www.elsevier.com/locate/ijhmt

The effects of bottom wall heating on mixed convection of yield stress fluids in cylindrical enclosures with a rotating end wall

Osman Turan [a,b,*], Nilanjan Chakraborty [b]

[a] Department of Mechanical Engineering, Bursa Technical University, Bursa 16310, Turkey
[b] School of Mechanical and Systems Engineering, Newcastle University, Newcastle-Upon-Tyne NE1 7RU, UK

ARTICLE INFO

Article history:
Received 21 June 2017
Received in revised form 24 December 2017
Accepted 4 January 2018
Available online 7 March 2018

Keywords:
Mixed convection
Bingham fluid
Rotating end wall
Reynolds number
Prandtl number
Richardson number
Bingham number

ABSTRACT

Steady-state laminar mixed convection of Bingham fluids in cylindrical enclosures with a rotating top cover has been numerically analysed for the configuration where the bottom cover is kept at a higher temperature than the rotating top cover. The numerical investigations have been carried out based on steady-state axisymmetric incompressible flow simulations for a range of different values Reynolds, Richardson, and Prandtl number given by $500 \leqslant Re \leqslant 3000$, $0 \leqslant Ri \leqslant 1$ and $10 \leqslant Pr \leqslant 500$ respectively. The aspect ratio (i.e. height: radius = $AR = H/R$) of the cylindrical container is considered to be unity (i.e. $AR = H/R = 1$). The mean Nusselt number $\overline{Nu}$ has been found to decrease sharply with increasing Bn owing to flow resistance arising from yield stress, but subsequently $\overline{Nu}$ asymptotically approaches a value of unity, which is indicative of a conduction-driven transport. In addition, the mean Nusselt number $\overline{Nu}$ has been found to increase with increasing Reynolds number due to the strengthening of advective transport. However, the mean Nusselt number $\overline{Nu}$ exhibits a non-monotonic trend (i.e. increases with increasing Ri for small values of Richardson number before showing a weak decreasing trend) with increasing Ri for Newtonian fluid (i.e. $Bn = 0$), whereas $\overline{Nu}$ increases with increasing Ri for small values of Richardson number before becoming a weak function of Ri for Bingham fluids. A step change in the mean Nusselt number has also been observed with an increase in Richardson number for some Bingham number values due to a change in flow pattern. The influences of Prandtl, Reynolds, Richardson, and Bingham numbers on the mean Nusselt number have been explained in detail based on both physical and scaling arguments. The simulation data and scaling relations have been utilised to propose a correlation for the mean Nusselt number, which has been shown to capture the numerical findings satisfactorily for the parameter range considered here.

1. Introduction

The swirling flow produced by rotating one of the end walls of cylindrical enclosures has several engineering applications (e.g. chemical processing, bio-chemical synthesis, polymer processing, food preparation, applications involving magneto-rheological and electro-rheological fluids etc.) for the purpose of augmenting the rate of heat transfer and mixing at relatively small values of Reynolds number. Flows of Newtonian fluids (where the viscous stress is directly proportional to the strain rate) in cylindrical enclosures with a rotating end cover have been extensively analysed in the existing literature [1–9]. The analysis of swirling flows in this configuration for Newtonian fluids was pioneered by the seminal experimental investigations by Vogel [1,2], Ronnenberg [3], Bertela and Gori [4], and these analyses reported vortical fluid motion within the enclosure as a result of the rotation of an end cover. The findings of these analyses [1–4] have subsequently been extended by Escudier [5] who used experimental investigation to demarcate the stability criterion for vortex breakdown in this configuration in terms of aspect ratio (i.e. height to radius ratio H/R) and Reynolds number $\Omega R^2/\nu$ (where Ω is the angular speed and ν is the kinematic viscosity). In addition to these experimental studies, several authors [6–9] numerically investigated this configuration for Newtonian fluids. Lee and Hyun [8] analysed the effects of Prandtl number on heat transfer rate in this configuration and reported significant Prandtl number dependence of the mean Nusselt number in this configuration. Iwatsu [9] analysed the effects of Reynolds and Richardson numbers (in the range of $100 \leqslant Re \leqslant 3000$ and $0 \leqslant Ri \leqslant 1$ for $Pr = 1$) on the flow pattern and heat transfer rate for swirling Newtonian fluid flows in a

* Corresponding author at: Department of Mechanical Engineering, Bursa Technical University, Bursa 16310 Turkey.
E-mail address: osman.turan@btu.edu.tr (O. Turan).

https://doi.org/10.1016/j.ijheatmasstransfer.2018.01.016
0017-9310/

Nomenclature

a	bridging function [-]
a_1, a_2	correlation parameters [-]
AR	aspect ratio, (AR = H/R) [-]
b	bridging function [-]
b_1, b_2	correlation parameters [-]
Bn	Bingham number [-]
c_p	specific heat at constant pressure [J/kg K]
C_T	torque coefficient [-]
e	relative error [-]
Ec	Eckert number [-]
g	gravitational acceleration [m/s^2]
Gr	Grashof number [-]
h	heat transfer coefficient [W/m^2 K]
H	height of cylindrical enclosure [m]
k	thermal conductivity [W/m K]
k_0,k_1	correlation parameters [-]
m_0,m_1	correlation parameters [-]
Nu	Nusselt number [-]
$\overline{Nu}$	mean Nusselt number [-]
Pr	Prandtl number [-]
q	heat flux [W/m^2]
R	radius of cylindrical enclosure [m]
Ra	Rayleigh number [-]
Re	Reynolds number [-]
Ri	Richardson number [-]
T	temperature [K]
U	characteristic velocity scales in radial direction (m/s)
V	characteristic velocity scales in tangential direction (m/s)
V_ϕ	non-dimensional swirl velocity, ($V_\phi = \upsilon H/\alpha$) [-]
α	thermal diffusivity [m^2/s]
β	coefficient of thermal expansion [1/K]
$\dot{\gamma}$	shear rate [1/s]
δ,δ_{th}	hydrodynamic and thermal boundary layer thickness [m]
θ	non-dimensional temperature, ($\theta = (T - T_C)/(T_H - T_C)$) [-]
μ	plastic viscosity [Ns/m^2]
μ_{yield}	yield viscosity [Ns/m^2]
υ	kinematic viscosity [m^2/s]
ρ	density [kg/m^3]
τ	shear stress [N/m^2]
τ_y	yield stress [N/m^2]
ϕ	general primitive variable [-]
$\boldsymbol{\Omega}$	angular velocity [1/s]
Ψ	stream function [m^2/s]
Ψ	non-dimensional stream function, ($\Psi = \psi/\alpha$) [-]

Subscripts

adv	advective
Bn = 0	Newtonian fluid case
C	cold wall
conv	convective
diff	diffusive
eff	effective value
H	hot wall
max	maximum value
r	radial direction
ref	reference value
wf	condition of the fluid in contact with the wall
z	axial direction
ϕ	tangential direction

Special characters

ΔT	difference between hot and cold wall temperature (= ($T_H - T_C$)) [K]
$\Delta_{\min,cell}$	minimum cell distance [m]
r	grid expansion ratio [-]

cylindrical enclosure with a heated rotating top wall for an aspect ratio of unity (i.e. $AR = H/R = 1$). The analysis by Iwatsu [9] revealed that advective transport weakens, whereas diffusive transport strengthens with an increase in Richardson number. All the aforementioned analyses were carried out for Newtonian fluids but heat transfer characteristics of yield stress fluids (i.e. fluids which flow only when a certain stress level is surpassed) in cylindrical enclosures with a rotating end wall received relatively limited attention in the existing literature despite its wide range of applications in chemical and food processing. Most analyses on the non-Newtonian fluid flow in cylindrical enclosures with a rotating cover were carried out for viscoelastic fluids [10,11]. Escudier and Cullen [10] experimentally analysed cylindrical enclosures with a rotating top cover for shear-thinning viscoelastic fluids, and reported that the vortex structure is different from the Newtonian fluid case and an intense toroidal vortex in the vicinity of the rotating cover drives a secondary low intensity vortex. Stokes and Boger [11] proposed a regime diagram for flow stability based on Reynolds and Elasticity numbers for viscoelastic fluids in cylindrical enclosures with a rotating cover. A recent experimental analysis of heat transfer under 'elastic turbulence' of viscoelastic fluids within cylindrical enclosures with a rotating top cover was reported by Traore et al. [12]. It was found by Traore et al. [12] that the heat transfer rate under elastic turbulence might locally increase up to 4 times in comparison to the value in the purely conduction regime due to the secondary irregular motion induced by elastic instabilities in polymer flow with large relaxation times. The influence of shear-thinning on vortex breakdown (observed by Vogel [1,2] and Escudier [5] for Newtonian fluids in the past) in cylindrical enclosures with a rotating cover was experimentally and numerically analysed for non-Newtonian fluids by Böhme et al. [13] where the viscosity was approximated by a power-law in terms of shear rate. Böhme et al. [13] constructed an aspect ratio - Reynolds number (AR - Re) diagram, representing the domain of vortex breakdown for shear-thinning fluids. A few analyses [14–16] have recently concentrated on the rotating disk configuration for yield stress fluids. The mass transfer of yield stress fluids in such applications has recently been investigated by Rashaida et al. [14] and semi-analytical approaches for analysing swirling flow of Bingham fluids over a rotating disk have been proposed by Ahmadpour and Sadegyhy [15] and Guha and Sengupta [16]. However, to date, a recent paper of the present authors [17] is only one paper in the existing literature which deals with both fluid flow and heat transfer characteristics of yield stress fluids in cylindrical enclosures with a rotating heated top wall in spite of its application in many chemical and food industries. Turan et al. [17] have numerically analysed mixed convection of Bingham fluids in cylindrical enclosures with a heated rotating top cover for an aspect ratio (height/radius) of unity (i.e. $AR = 1$) for a range of different values of nominal Prandtl, Richardson and Reynolds numbers given by $10 < Pr < 500$, $0 < Ri < 1$ and $100 < Re < 3000$.

It is possible to have four different configurations for cylindrical enclosures with a rotating end wall which are schematically shown in Fig. 1. A careful analysis of these four configurations

(i.e. C1–C4 configurations) reveals that the C3 and C4 configurations are equivalent to the C1 and C2 configurations respectively from the point of view of both fluid dynamics and heat transfer. It is indeed confirmed by the present authors that both rotating top and bottom cover configurations yield the same numerical value of the mean Nusselt number ($\overline{Nu}$) when the thermal boundary conditions are kept unaltered which indicates that heat transfer rate for a given set of thermal boundary conditions remains insensitive to the orientation of the rotating end wall. For this reason, only two main configurations, C1 and C2 are sufficient for heat transfer analysis. Turan et al. [17] have recently dealt with the C1 configuration but the C2 configuration is yet to be analysed in detail. It is worth noting that the C2 configuration is fundamentally different from the C1 configuration. In the C1 configuration, the lighter hot fluid adjacent to the heated top wall sits on top of the heavier cold fluid and thus represents a stable stratified condition. By contrast, the C2 configuration represents an unstable condition where the heavier cold fluid sits on top of the lighter hot fluid adjacent to the heated bottom wall. Thus, both flow structure and heat transfer characteristics in the C2 configuration are likely to be different from those in the C1 configuration. In this paper, a detailed parametric analysis has been conducted to analyse the effects of yield stress on heat and momentum transport for a range of different nominal values of Richardson, Reynolds and Prandtl numbers (definitions are provided in Section 2). The present analysis concentrates on the steady-state analysis of mixed convection and it was demonstrated by Iwatsu [9] that steady-state axisymmetric solutions for Newtonian fluids (i.e. $Bn = 0$) can be obtained for the Reynolds number and Richardson number ranges given by $500 \leqslant Re \leqslant 3000$ and $0 \leqslant Ri \leqslant 1$. The effective values of Reynolds number in the Bingham fluid cases are expected to be smaller than in the corresponding Newtonian fluid cases and thus steady-state axisymmetric solutions are expected to be valid for the ranges of nominal values of Reynolds number and Richardson number given by: $500 \leqslant Re \leqslant 3000$ and $0 \leqslant Ri \leqslant 1$. The nominal Prandtl number range given by $10 \leqslant Pr \leqslant 500$ has been considered here for the purpose of numerical experimentation because practical yield stress fluids (e.g. Carbopol) exhibit Prandtl numbers of the order of 100 [18,19], whereas the Prandtl number of water remains of the order of 10. The flow is likely to be three-dimensional and the assumption of axisymmetry is unlikely to be valid for $Re \gg 3000$ and $Ri \gg 1$, and three-dimensional simulations of Bingham fluids in this configuration is about 20–30 times more expensive than two-dimensional axisymmetric simulations depending on the Bingham number Bn. Thus, it is impractical to conduct a parametric analysis in terms of Re, Ri, Pr and Bn for the ranges of aforementioned non-dimensional numbers considered here based on three-dimensional simulations.

The rest of the articles will be organised as follows. The necessary mathematical background and numerical implementation will be discussed in the next section. Following this, results will be presented and subsequently discussed. The main findings are summarized and conclusions are drawn in the final section.

2. Mathematical background & numerical implementation

2.1. Constitutive equations

Many empirical models have been proposed in existing literature for describing the interrelation between shear stress and strain rate in yield-stress fluids. In this study, the Bingham model [20] is used, which is the simplest model to describe the relationship between shear stress and strain rate in yield stress fluids. The mathematical expression of the Bingham model is given as:

$$\underline{\underline{\dot{\gamma}}} = 0 \quad \text{for} \quad \tau \leqslant \tau_y \tag{1}$$

$$\underline{\underline{\tau}} = \left(\mu + \frac{\tau_y}{\dot{\gamma}}\right)\underline{\underline{\dot{\gamma}}} \quad \text{for} \quad \tau > \tau_y \tag{2}$$

where $\underline{\underline{\dot{\gamma}}}$ and $\underline{\underline{\tau}}$ are the tensor of the strain rate and shear stress respectively, τ_y is the yield stress and μ is the so-called plastic viscosity of the yielded fluid. The quantities τ and $\dot{\gamma}$ are defined based on the second invariants of the stress and the rate of strain tensors, respectively:

$$\tau = \left[\frac{1}{2}\underline{\underline{\tau}} : \underline{\underline{\tau}}\right]^{1/2} \tag{3}$$

$$\dot{\gamma} = \left[\frac{1}{2}\underline{\underline{\dot{\gamma}}} : \underline{\underline{\dot{\gamma}}}\right]^{1/2} \tag{4}$$

O'Donovan and Tanner [21] used the bi-viscosity model to mimic the stress-shear rate characteristics for a Bingham fluid in the following manner:

$$\underline{\underline{\tau}} = \mu_{yield}\underline{\underline{\dot{\gamma}}} \quad \text{for} \quad \dot{\gamma} \leqslant \frac{\tau_y}{\mu_{yield}} \tag{5}$$

$$\underline{\underline{\tau}} = \tau_y + \mu\left[\underline{\underline{\dot{\gamma}}} - \frac{\tau_y}{\mu_{yield}}\right] \quad \text{for} \quad \dot{\gamma} > \frac{\tau_y}{\mu_{yield}} \tag{6}$$

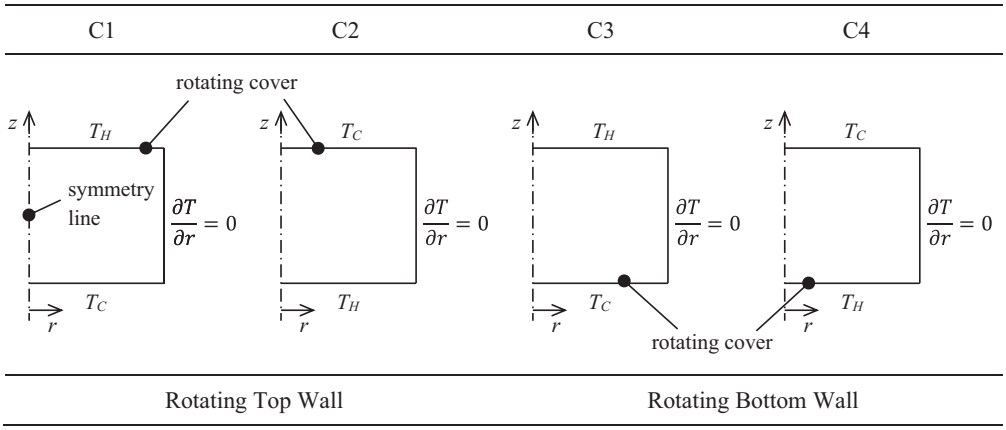

Fig. 1. Schematic diagrams of the simulation domain and different boundary conditions where T_H and T_C are the hot and cold wall temperatures.

where μ_{yield} is the yield viscosity. The bi-viscosity regularisation replaces the unyielded regions by a region of very high viscosity. A large value of μ_{yield}/μ needs to be chosen to replicate the Bingham model. The sensitivity of the choice of μ_{yield}/μ in the case of mixed convection of Bingham fluids in cylindrical enclosures with a rotating end wall has been analysed by Turan et al. [17] and they suggested a value of $\mu_{yield}/\mu = 10^8$ for ensuring high-fidelity of the simulations. Accordingly, $\mu_{yield}/\mu = 10^8$ has been chosen for the present analysis.

2.2. Governing equations and boundary conditions

For the present analysis, a steady-state laminar incompressible axisymmetric swirling flow is considered. Under this condition the conservation equations in the cylindrical coordinate system take the following form:

Mass conservation equation

$$\frac{\partial u}{\partial r} + \frac{u}{r} + \frac{\partial w}{\partial z} = 0 \tag{7}$$

Momentum conservation equations

$$\rho\left(u\frac{\partial u}{\partial r} - \frac{v^2}{r} + w\frac{\partial u}{\partial z}\right) = -\frac{\partial p}{\partial r} + \frac{\partial \tau_{zr}}{\partial z} + \frac{\partial \tau_{rr}}{\partial r} + \frac{\tau_{rr} - \tau_{\phi\phi}}{r} \tag{8a}$$

$$\rho\left(u\frac{\partial v}{\partial r} + \frac{uv}{r} + w\frac{\partial v}{\partial z}\right) = \frac{\partial \tau_{r\phi}}{\partial r} + \frac{\partial \tau_{z\phi}}{\partial z} + \frac{2\tau_{r\phi}}{r} \tag{8b}$$

$$\rho\left(u\frac{\partial w}{\partial r} + w\frac{\partial w}{\partial z}\right) = -\frac{\partial p}{\partial z} + \rho g\beta(T - T_{ref}) + \frac{1}{r}\frac{\partial}{\partial r}(r\tau_{rz}) + \frac{\partial \tau_{zz}}{\partial z} \tag{8c}$$

Energy conservation equation

$$\rho c_p\left(u\frac{\partial T}{\partial r} + w\frac{\partial T}{\partial z}\right) = k\left(\frac{1}{r}\frac{\partial T}{\partial r} + \frac{\partial^2 T}{\partial r^2} + \frac{\partial^2 T}{\partial z^2}\right) \tag{9}$$

where u, v and w are the velocity components in radial (i.e. r), tangential (i.e. ϕ) and axial (i.e. z here vertical direction) directions, respectively, ρ is the fluid density, p is the pressure, T is the temperature, T_{ref} is the reference temperature for evaluating the buoyancy term $\rho g\beta(T - T_{ref})$ in the momentum conservation equation in the vertical direction, and here T_{ref} is taken to be the cold wall temperature T_c, g is the acceleration due to gravity, and β is the volume expansion coefficient. In addition, thermo-physical properties (thermal conductivity k, specific heat c_p, plastic viscosity μ, yield-stress τ_y etc.) are assumed to be constant and independent of temperature in this analysis for the sake of simplicity. The aspect ratio ($AR = H/R$) of the cylindrical container is considered to be unity (i.e. $AR = H/R = 1$). The bottom and top covers of the cylindrical enclosure are kept at different temperatures ($T_C < T_H$), while the cylindrical circumferential surface is considered to be adiabatic. The temperature difference between the top and bottom covers are considered small enough to ensure that the Boussinesq approximation remains valid. For typical thermo-physical properties of yield stress fluids (see Table 1 of Ref. [19]), one needs a very large value of ΩR (to be realised in process engineering applications) to obtain large values of Eckert number $Ec = \Omega^2 R^2/c_p\Delta T$, which leads to strong viscous dissipation effects in the energy conservation equation. Thus, the viscous dissipation effects in Eq. (9) are neglected without much loss of generality in this analysis. The velocity components are identically zero due to no-slip condition and impenetrability on the surface of the container. Symmetry boundary condition is imposed for the axis.

2.3. Non-dimensional numbers

In the case of mixed convection for Bingham fluids the Nusselt number Nu is expected to be dependent on Reynolds, Richardson, Prandtl and Bingham numbers (i.e. Re, Ri, Pr and Bn) according to the Buckingham's pi theorem. Here, Re, Ri, Pr, Bn and Nu are defined in the following manner according to the previous analysis by Turan et al. [17]:

$$Re = \frac{\rho\Omega R^2}{\mu};\ Ri = \frac{Gr}{Re^2} = \frac{g\beta\Delta TH^3}{\Omega^2 R^4};\ Gr = \frac{\rho^2 g\beta\Delta TH^3}{\mu^2};\ Pr = \frac{\mu c_p}{k};$$
$$Bn = \frac{\tau_y}{\mu\Omega};\ Nu = \frac{hR}{k} \tag{10}$$

where the heat transfer coefficient h is defined as:

$$h = \left| -k\frac{\partial T}{\partial z}\bigg|_{wf} \times \frac{1}{T_{wall} - T_{ref}} \right| \tag{11}$$

Here the subscript 'wf' refers to the condition of the fluid in contact with the wall, T_{wall} is the wall temperature and T_{ref} is the appropriate reference temperature, which can be taken to be $T_C(T_H)$ for the hot (cold) wall. It is also worth noting that viscosity varies throughout the domain for Bingham fluid flows and thus, an effective viscosity can be expressed as: $\mu_{eff} = \tau_y/\dot{\gamma} + \mu$, which might be more representative of the viscous action within the flow than the constant plastic viscosity μ. Therefore, the non-dimensional numbers could have been defined more appropriately if μ_{eff} was used instead of μ. However, $\dot{\gamma}$ is expected to show local variations in the flow domain so using a single characteristic value in the definitions of the non-dimensional numbers is unlikely to offer any additional benefit in comparison to the nominal definitions [17].

In the present study, the thermo-physical properties such as thermal conductivity k, specific heat c_p, plastic viscosity μ and yield stress τ_y are taken to be independent of temperature for the sake of simplicity and also for the purpose of generalisation. Moreover, experimental evidence suggests that the yield stress remains approximately independent of temperature and the plastic viscosity is only a weakly decreasing function of temperature (similar to Newtonian fluids) for a well-known yield stress fluid Carbopol in the temperature range 0–90 °C [22]. Thus, the simulation outcomes for temperature-dependent physical properties are likely to be qualitatively similar to those with constant thermo-physical properties.

2.4. Numerical implementation, grid-independency, and benchmarking

In this study, a commercial package ANSYS-FLUENT, which was utilised previously successfully for the simulations of both non-Newtonian [23] and Newtonian fluids [24], has been used in order to solve the conservation equations of mass, momentum, and energy in a framework of finite-volume technique. For this analysis, a second-order central difference technique is used for the discretisation of the diffusive terms and a second-order upwind scheme is used for the convective terms. Coupling of pressure and velocity is achieved using the well-known SIMPLE (Semi-Implicit Method for Pressure-Linked Equations) algorithm [25]. The convergence criteria in FLUENT were set to 10^{-7} for all the relative (scaled) residuals. Interested readers are referred to Turan et al. [17] for further discussion on the choice of convergence criterion.

Three different non-uniform meshes M1 (50×50), M2 (100×100) and M3 (200×200) have been investigated for the purpose of grid sensitivity analysis, and the details of these meshes have been provided in Table 1 where the normalised minimum grid spacing $\Delta_{min,cell}/R$ and grid expansion ratio r_e are provided. The numerical uncertainty for the mean Nusselt number (i.e. $\overline{Nu} = \int_0^R Nu 2\pi r dr/\pi R^2$) in the case of Newtonian (i.e. $Bn = 0$) flow and a representative Bingham fluid flow (i.e. $Bn = 2.0$) case for Re = 1000 and $Ri = 0.1$ at $Pr = 100$ are shown in Table 1. Table 1 highlights that the maximum relative error levels (e_a) between M2 (100×100) and M3 (200×200) are under 1% for both Bingham and Newtonian fluids. Based on this analysis, the simulations have been conducted using mesh M2 (100×100), which is found to be sufficient for providing high accuracy and computational efficiency. In addition to the grid-independency study, the simulation results for Newtonian fluids have also been compared with respect to the data reported by Iwatsu [9] in the case of C1 configuration and an excellent agreement was obtained. Interested readers are referred to Turan et al. [17] for further information on benchmarking with respect to the numerical data by Iwatsu [9]. The numerical scheme used here has previously been validated earlier for laminar natural convection of Bingham fluids in square enclosures, and interested readers are referred to Turan et al. [26] for further information in this regard.

2.5. Scaling analysis

Turan et al. [17] carried out a detailed scaling analysis to elucidate the influences of Reynolds, Richardson, Rayleigh, Prandtl and Bingham numbers on the mean Nusselt number in the C1 configuration. The same scaling analysis also applies to the C2 configuration and thus is not repeated here. The key results of this scaling analysis are summarised in Table 2. Interested readers are referred to Turan et al. [17] for further discussion on the derivation of these scaling relations.

Table 2
Summary of the important results of the scaling analysis reported by Turan et al. [17].

The balance between inertial and viscous forces		$\rho \frac{V^2}{R} \sim \frac{\tau}{\delta}$
Velocity scales		$V \sim \Omega R$
		$U \sim a(\Omega R) + b(\sqrt{g\beta\Delta T R})$
		where $a = e^{-Ri}$ and $b = 1 - e^{-Ri}$
Shear stress		$\tau \sim \tau_y + \mu(U/\delta)$
Hydrodynamic boundary layer thickness		$\frac{\delta}{R} \sim \frac{Bn}{2Re} + \frac{1}{2Re}\sqrt{Bn^2 + 4\left[aRe + b\left(\frac{Ra}{Pr}\right)^{1/2}\right]}$
Nusselt number scale[a]		$\overline{Nu} \sim \frac{2Re}{Bn+\sqrt{Bn^2+4\left[aRe+b\left(\frac{Ra}{Pr}\right)^{1/2}\right]}} f_1$
$Bn \neq 0$	$Ri = 0$	$\overline{Nu} \sim \frac{2Re}{Bn+\sqrt{Bn^2+4Re}} f_1$
	$Ri \gg 1$	$\overline{Nu} \sim \frac{2Re}{Bn+\sqrt{Bn^2+4\left(\frac{Ra}{Pr}\right)^{1/2}}} f_1$
$Bn = 0$	$Ri = 0$	$\overline{Nu} \sim Re^{1/2} f_1$
	$Ri \gg 1$	$\overline{Nu} \sim Ri^{-1/2}(Ra/Pr)^{1/4} f_1 = (Ra/Pr)^{1/4} f_2$

[a] Nusselt number can be scaled as: $\overline{Nu} = hR/k \sim R/\delta_{th} \sim (R/\delta) f_1(Re, Ri, Ra, Pr, Bn)$ where f_i is a function of Re, Ri, Ra, Pr and Bn, which accounts for the ratio of hydrodynamic to thermal boundary layer thicknesses (i.e. $\delta/\delta_{th} \sim f_1(Re, Ri, Ra, Pr, Bn)$).

3. Results & discussions

It is worth noting that the influences of Bn, Re, Ri and Pr on the mean Nusselt number $\overline{Nu}$ are interrelated but it is not helpful from the point of view of fundamental understanding to show the variations of $\overline{Nu}$ with simultaneous changes of the aforementioned non-dimensional parameters. Thus, the variations of $\overline{Nu}$ in response to the change in one key parameter when other parameters are unaltered are discussed in Sections 3.1–3.4 solely for the convenience of presenting the results and their discussion.

3.1. Variations of Bingham number

The variations of the mean Nusselt number $\overline{Nu}$ with the changes in Bingham number Bn are shown in Fig. 2 for $Re = 500, 1000$ and 2000 at $Ri = 0.1$ and $Pr = 100$. For the purpose of numerical experimentation, the range of Bingham number is chosen in such a manner that the mean Nusselt number $\overline{Nu}$ approaches the value obtained for pure conduction for the highest value of Bn considered here. It is worth noting that the Bingham number $Bn = \tau_y/\mu\Omega$ can be modified by changing the angular speed Ω and for electro-rheological and magneto-rheological fluids the yield stress τ_y can be modified by applying electrical and magnetic fields to obtain a desired value of Bn. In order to elucidate the behaviour at high values of Bingham number, the variations of $\overline{Nu}$ with $Bn^* = \log(Bn^2 + 1)$ are shown in Fig. 2. It is evident from Fig. 2 that $\overline{Nu}$ decreases sharply with increasing Bn, and eventually approaches asymptotically to a value of unity, which is indicative of a conduction-driven transport. It is worth noting that the variation of $\overline{Nu}$ with Bn^* shown in Fig. 2 is consistent with the scaling estimate shown in Table 2, which indicates a decreasing trend of $\overline{Nu}$ with increasing Bn. It is shown in Fig. 2 that the contours of non-dimensional temperature $\theta = (T - T_C)/(T_H - T_C)$ are curved and not parallel to horizontal walls, especially in the vicinity of the cold rotating cover, even for $\overline{Nu} = 1.001$, which suggests that the effects of advective transport sustain even for small values of mean Nusselt number in this configuration. Therefore, in this study, the criterion for the fully conduction-dominated regime is taken to be $\overline{Nu} = 1.0001$ because the isotherms for this condition remain parallel to the horizontal walls as predicted by a pure-conduction solution. It can be seen from Fig. 2 that viscous resistance strengthens in comparison to buoyancy and inertial forces with increasing Bn for mixed convection (e.g. $Ri = 0.1$).

Table 1
The details of the meshes and the relative error for the mean Nusselt number $\overline{Nu}$ for Newtonian (i.e. $Bn = 0$) and Bingham fluids (e.g. $Bn = 2$) for $Ri = 0.1$ and $Re = 1000$ at $Pr = 100 <!--Queryid = Q5 desc = Pleasecheckthelayoutandeditsmade in Tables 14, and correct if necessary./-->$.

Mesh Details	M1 (50×50)	M2[a] (100×100)	M3 (200×200)
$\Delta_{min,cell}/R$	3.10×10^{-3}	1.55×10^{-3}	0.78×10^{-3}
r_e	1.0630	1.0307	1.0152
Relative Error	M1 (50×50)	M2[a] (100×100)	M3 (200×200)
$\overline{Nu}$ ($Bn = 0$)	32.8294	32.2667	32.0751
e_a (%)	1.7140	0.5938	
$\overline{Nu}$ ($Bn = 2$)	6.4067	6.4440	6.4685
e_a (%)	0.5822	0.3802	

[a] The mesh which is used for the numerical simulations.

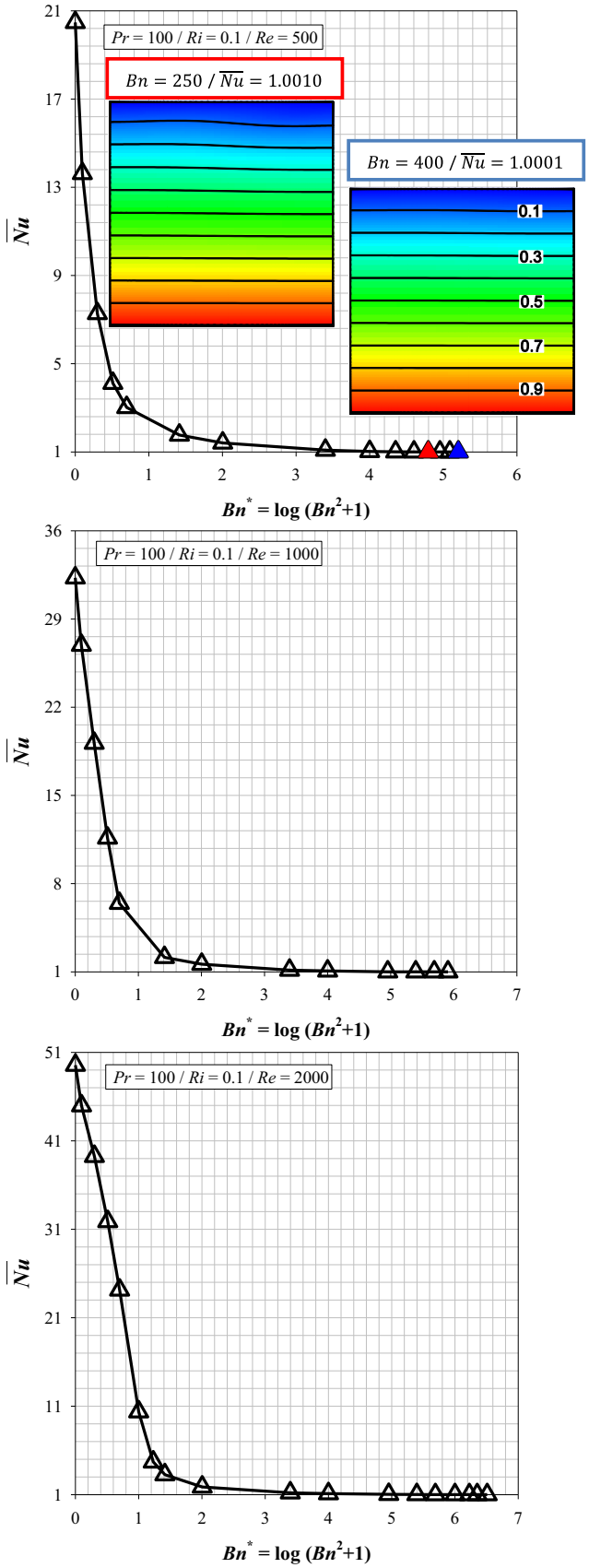

Fig. 2. The variation of mean Nusselt number $\overline{Nu}$ with Bingham number Bn for different values of Reynolds number Re for $Ri = 0.1$ and $Pr = 100$.

As in the previous study [17], the Bingham number at which the mean Nusselt number approaches 1.0001 is referred to Bn_{max} in this paper. This suggests that $1.0 \leqslant \overline{Nu} \leqslant 1.0001$ for $Bn \geqslant Bn_{max}$ and $\overline{Nu} > 1.0001$ for $0 < Bn < Bn_{max}$. For large values of Bingham number, the fluid flow becomes too weak to impart any influence on thermal transport and heat transfer takes place due to conduction. Under conduction heat transfer, both C1 and C2 configurations become equivalent to each other. Thus, Bn_{max} is found to be the same for both C1 and C2 configurations. This can be verified from Fig. 3 which shows that Bn_{max} values for the C2 configuration are exactly the same as those in the C1 configuration (as reported by Turan et al. [17]). Using the mean Nusselt number scaling in Table 2, one can estimate Bn_{max} as [17]:

$$Bn_{max} \sim Ref_1 - (a + bRi^{0.5})/f_1 \tag{12}$$

Eq. (12) suggests that Bn_{max} increases with increasing Re. The advective transport strengthens with increasing Re and as a result the Bingham number at which $\overline{Nu}$ approaches to 1.0001 (i.e. $Bn = Bn_{max}$) increases with increasing Re. It is worth noting that the function f_1 represents the ratio of thicknesses of hydrodynamic and thermal boundary layers, and this ratio increases with increasing Pr. Thus, the numerical value of Bn_{max} is expected to increase with increasing Pr. Fig. 3 indeed shows that Bn_{max} increases with increasing Re and Pr, whereas Bn_{max} is not significantly influenced by Ri. Turan et al. [17] parameterised Bn_{max} as $Bn_{max} = 0.04Re^{1.08}Pr^{0.57}$ for the C1 configuration, which is valid also for the C2 configuration. It is worth noting that the Bn_{max} correlation should be treated with caution because $\overline{Nu} = 1.0001$ is not equivalent to the critical condition under which flow stops in the enclosure. In the context of bi-viscosity regularisation, the flow does not stop in a true sense for $Bn \geqslant Bn_{max}$, but it becomes extremely weak to influence the thermal transport. The critical condition in terms of Bingham number for which flow stops is not necessary from the perspective of heat transfer analysis conducted here.

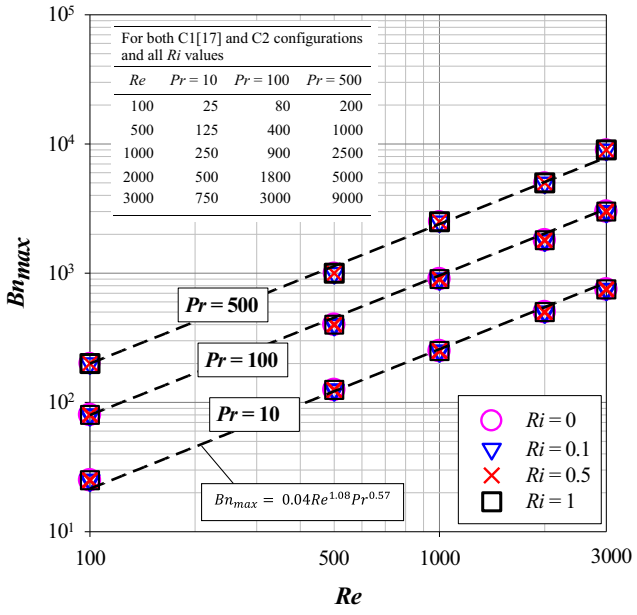

Fig. 3. The variation of Bn_{max} with Reynolds number Re for different values of Pr and Ri for both C1 and C2 configurations along with Bn_{max} correlation [17].

The weakening of thermal advective transport for large values of Bingham number can be substantiated from Fig. 4 where the contours of non-dimensional stream function $\Psi(=\psi/\alpha$ where ψ is the dimensional stream function and $\alpha = k/\rho c_p$ is the thermal diffusivity) and non-dimensional temperature $(\theta = (T - T_C)/(T_H - T_C))$ are shown for different values of Bn at $Re = 1000$, $Ri = 0.1$, and $Pr = 100$. Fig. 4 shows a large region of uniform temperature especially for Newtonian (i.e. $Bn = 0$) fluid cases and also for small values of Bingham number (e.g. $Bn = 1$). A large region of uniform temperature, as observed in Fig. 4, indicates high rate of heat transfer. However, this region of uniform temperature distribution disappears with increasing Bn and the region of low

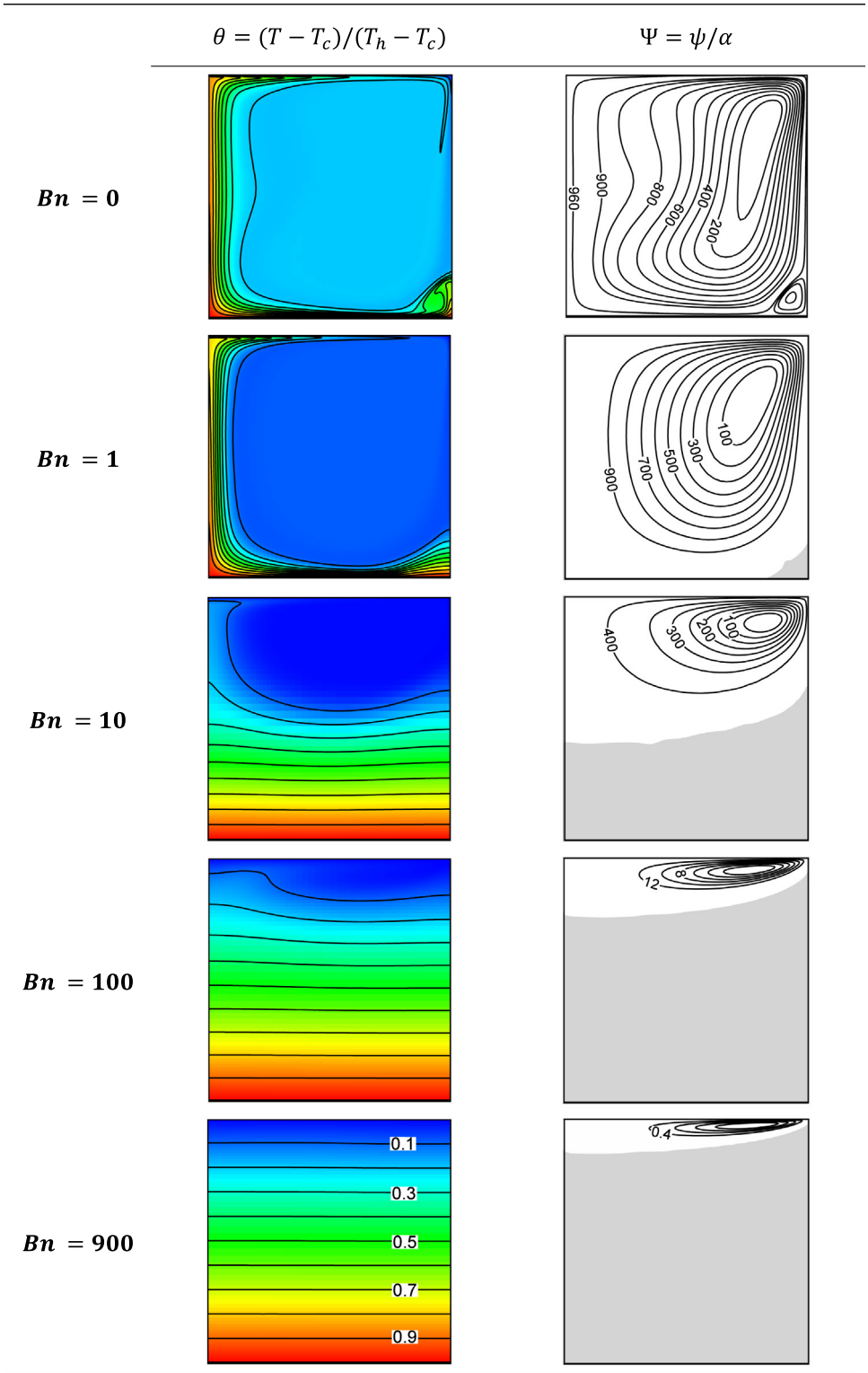

Fig. 4. The contours of non-dimensional temperature θ and stream function $\Psi = \psi/\alpha$ with AURs (shown in grey) for different values of Bn for $Ri = 0.1$ at $Re = 1000$ and $Pr = 100$.

temperature moves to the top of the container. The isotherms become increasingly parallel to the active covers (i.e. top and bottom covers) of the container with a gradual increase in temperature from the top to the bottom of the container (i.e. with a large thermal boundary layer) as the Bingham number increases. Moreover, the magnitude of Ψ decreases with increasing Bn which is indicative of the weakening of advective transport in the container. This behaviour is also indicative of the strengthening of conduction-driven transport with increasing Bn, and the heat transfer takes place principally due to conduction, when Bn reaches Bn_{max}.

It is also worth noting that the grey regions on the streamline plots in Fig. 4 indicate the Apparently Unyielded Regions (AURs) (regions where $|\tau| \leqslant \tau_y$ [27]). According to the bi-viscosity regularisation the unyielded zones are replaced by the regions of high viscosity– regions of extremely slowly moving fluid (Mitsoulis and Zisis [27] called them "apparently unyielded regions (AUR)"). In AURs, the flow becomes so weak (i.e. the magnitudes of velocity and stream function become negligible) that these regions can effectively be considered as stagnant zones. The velocity magnitudes in these zones are so small that they do not impart any influence on thermal transport. An idea about the locations of the unyielded zones can be obtained from the AURs. However, it is important to note that AURs are not really "unyielded" in the true sense in the context of bi-viscosity regularisation, as pointed out by Mitsoulis and Zisis [27].

3.2. Variations of Reynolds number

The variation of the mean Nusselt number $\overline{Nu}$ with nominal Reynolds number Re in the case of Newtonian (i.e. $Bn = 0$) fluids and representative Bingham fluid cases (i.e. $Bn = 2$ and 5) is shown in Fig. 5 for $Ri = 0.1$ and $Pr = 100$. Fig. 5 shows that $\overline{Nu}$ increases with increasing Re, which is also expected from the scaling estimate of the mean Nusselt number (see Table 2). An increase in Nusselt number with increasing Reynolds number is indicative of the strengthening of advective transport. This can be substantiated from Fig. 6 where the distributions of non-dimensional swirl velocity component V_ϕ $(= vH/\alpha)$ along the vertical mid-plane

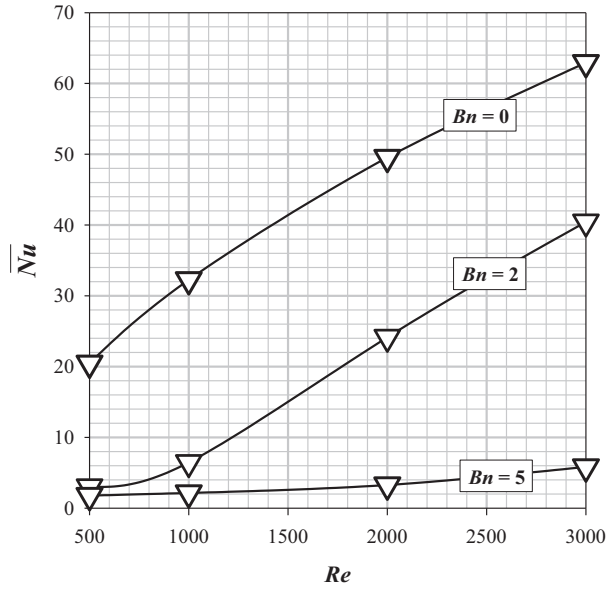

Fig. 5. The variation of mean Nusselt number $\overline{Nu}$ with Reynolds number Re in the case of Newtonian (i.e. $Bn = 0$) and Bingham (i.e. $Bn = 2$ and 5) fluids for $Ri = 0.1$ and $Pr = 100$.

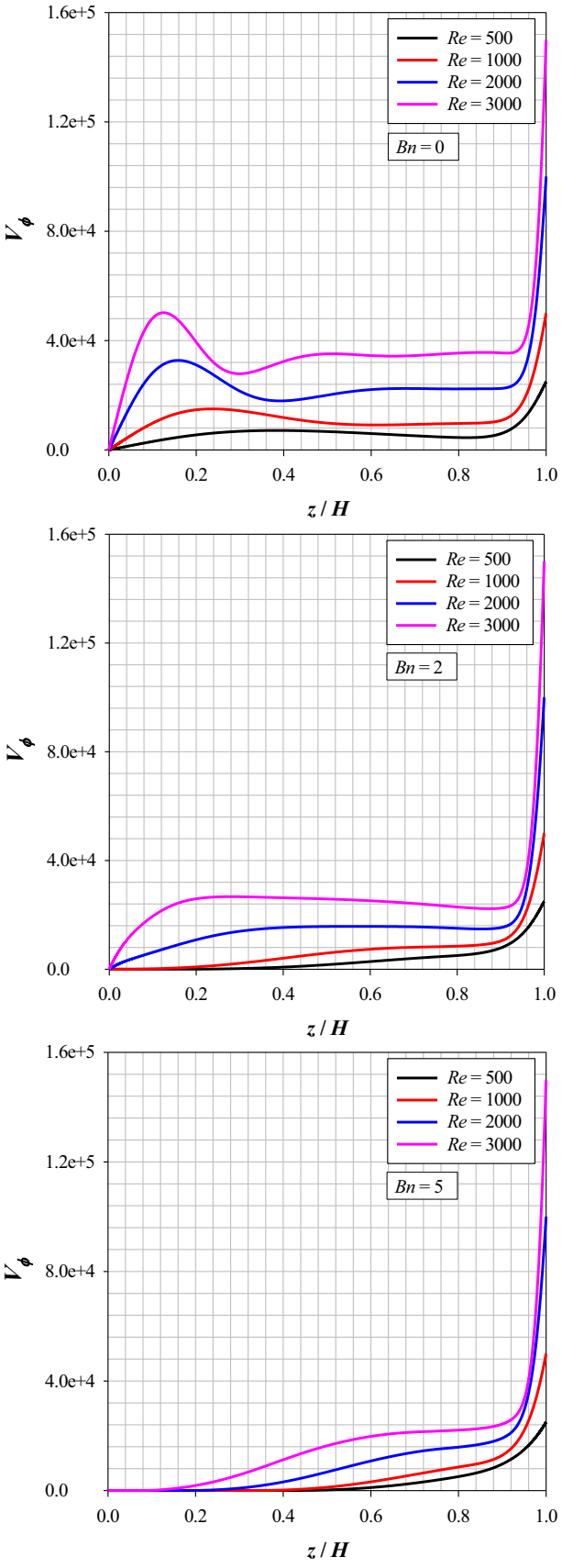

Fig. 6. The variation of non-dimensional swirl velocity component V_ϕ along the vertical mid-plane (i.e. $r/R = 0.5$) for different Reynolds number Re values for Newtonian (i.e. $Bn = 0$) and Bingham fluid (i.e. $Bn = 2$ and 5) cases at $Ri = 0.1$ and $Pr = 100$.

($r/R = 0.5$) are presented for both Newtonian (i.e. $Bn = 0$) and representative Bingham (for $Bn = 2$ and 5) fluid cases for different values Re at $Ri = 0.1$. It can be seen from Fig. 6 that the magnitude of V_ϕ increases with increasing Re for all Bn cases, which indicates the strengthening of thermal advection with an increase in Re.

The strengthening of advective transport with increasing Re could alternatively be explained by integrating convective heat transport through the boundary layer thickness on the bottom cover:

$$Q_{conv} = Q_{adv} + Q_{diff} = \int_0^\delta \rho c_p u \Delta T dz - \int_0^\delta k(\partial T/\partial r) dz \tag{13}$$

where

$$Q_{adv} = \int_0^\delta \rho c_p u \Delta T dz \sim \rho c_p U \Delta T \delta \tag{14a}$$

$$Q_{diff} = -\int_0^\delta k\left(\frac{\partial T}{\partial r}\right) dz \sim (k\Delta T)\frac{\delta}{R} \tag{14b}$$

where δ is the hydro-dynamic boundary layer thickness on the horizontal walls. Substituting $U \sim a(\Omega R) + b(\sqrt{g\beta\Delta TR})$ and the scaling relation for δ from Table 2 into Eqs. (14a) and (14b) yield the following scaling estimates for the magnitudes of Q_{adv} and Q_{diff}:

$$Q_{adv} \sim 0.5(k\Delta T)Pr[a + bRi^{1/2}]\left[Bn + \sqrt{Bn^2 + 4Re[a + bRi^{1/2}]}\right] \tag{15a}$$

$$Q_{diff} \sim 0.5(k\Delta T)\left[\frac{Bn}{Re} + \sqrt{\frac{Bn^2}{Re^2} + \frac{4}{Re}[a + bRi^{1/2}]}\right] \tag{15b}$$

Eqs. (15a) and (15b) indicate that the advective (diffusive) heat transport Q_{adv} strengthens (weakens) with increasing Re as evident from Figs. 5 and 6. For this reason, the mean Nusselt number $\overline{Nu}$ increases (decreases) with increasing (decreasing) Re, as shown in Fig. 5.

Figs. 5 and 6 also indicate that the influences of Reynolds number Re on the mean Nusselt number $\overline{Nu}$ weaken, and the magnitude of swirling velocity component V_ϕ decreases with increasing Bn. This can be explained in the following manner. In the case of Bingham fluids, an effective viscosity instead of a constant plastic viscosity would have been more appropriate while defining an

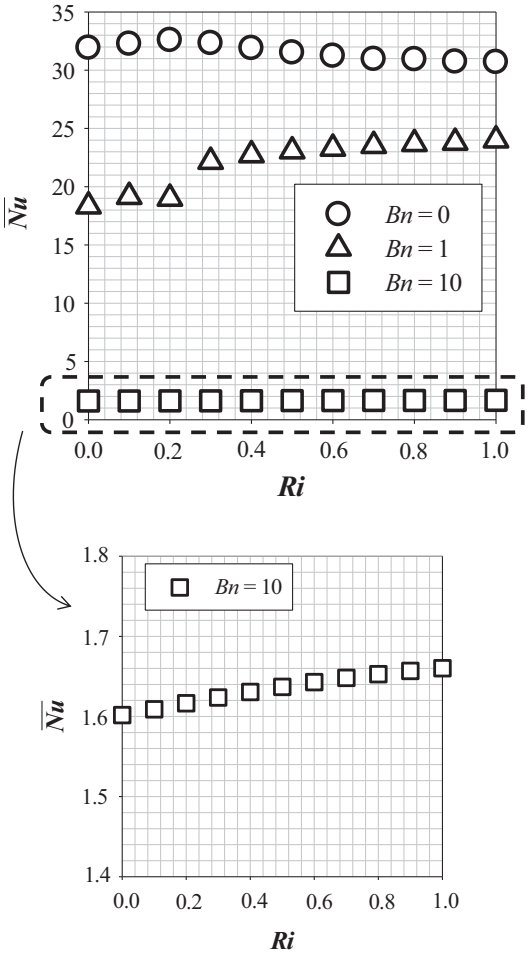

Fig. 7. The variation of mean Nusselt number $\overline{Nu}$ with Richardson number Ri and for different values of Bingham number Bn at Re = 1000 and Pr = 100.

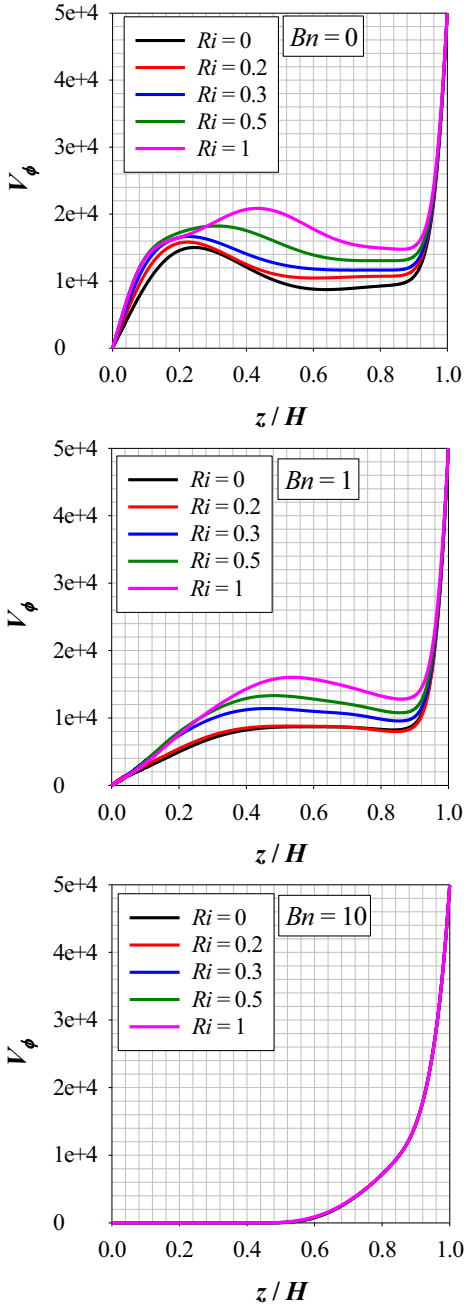

Fig. 8. The variation of the non-dimensional swirl velocity V_ϕ for different values of Bingham number Bn at Re = 1000 and Pr = 100.

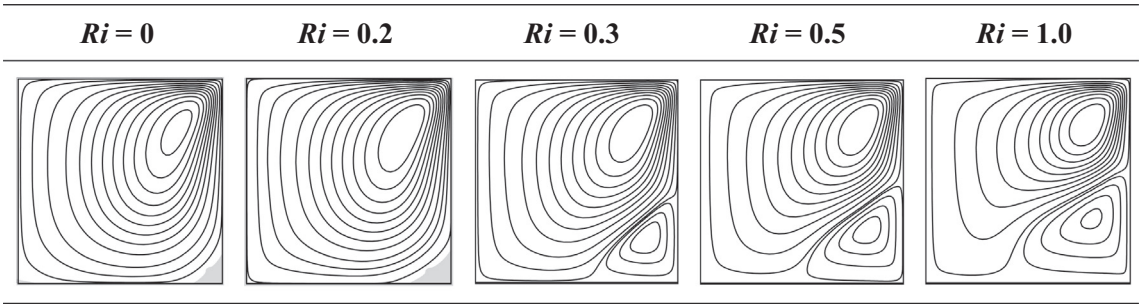

Fig. 9. The contour of non-dimensional stream function $\Psi = \psi/\alpha$ with AURs (shown in grey) at $Bn = 1$, $Re = 1000$ and $Pr = 100$.

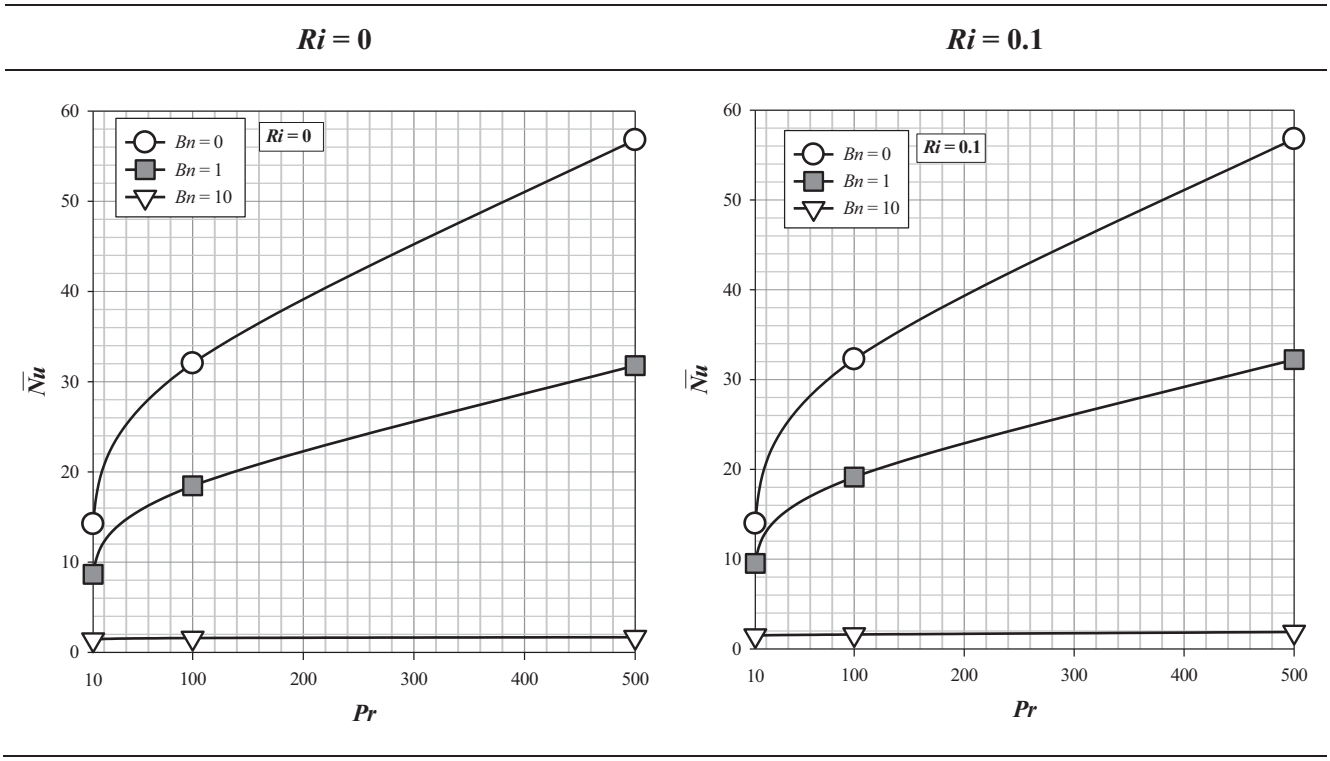

Fig. 10. The variation of mean Nusselt number $\overline{Nu}$ with Prandtl number Pr in the case of Newtonian (i.e. $Bn = 0$) and Bingham (i.e. $Bn = 1$ and 10) fluids for $Ri = 0$ (i.e. purely forced convection) and 0.1 (i.e. mixed convection) at $Re = 1000$.

effective Reynolds number. The "effective" viscosity can be estimated as:

$$\mu_{eff} \sim \tau_y/\dot{\gamma} + \mu \tag{16}$$

which can be scaled as:

$$\mu_{eff} \sim \tau_y \delta/U + \mu \tag{17}$$

Using scaling relation of δ from Table 2 and using the velocity scales $U \sim a(\Omega R) + b(\sqrt{g\beta\Delta TR})$ and $V \sim \Omega R$ lead to:

$$\mu_{eff} \sim \frac{\tau_y R}{a(\Omega R) + b\sqrt{g\beta\Delta TR}}\left(\frac{Bn}{2Re} + \frac{1}{2Re}\sqrt{Bn^2 + 4[aRe + bReRi^{1/2}]}\right) + \mu \tag{18}$$

Based on Eq. (18), an effective Reynolds number Re_{eff} can be defined as:

$$Re_{eff} = \frac{\rho\Omega R^2}{\mu_{eff}} = \frac{Re(a + bRi^{1/2})}{(a + bRi^{\frac{1}{2}}) + \left(\frac{Bn^2}{2Re} + \frac{Bn}{2Re}\sqrt{Bn^2 + 4[aRe + bReRi^{1/2}]}\right)} \tag{19}$$

Eq. (19) suggests that the effective Reynolds number Re_{eff} decreases with increasing Bn for a given set of values of Re and Ri, which is consistent with the weakening of thermal advection with an increase in Bn (see Figs. 5 and 6). Thus, an increase in Bn for a given set of values of Re and Ri leads to a drop of Re_{eff} and as a result the augmentation of advective transport with increasing Reynolds number is relatively weak for high values of Bn.

3.3. Variations of Richardson number

The variation $\overline{Nu}$ and non-dimensional swirl velocity component V_ϕ with Ri are presented in Figs. 7 and 8 respectively. It can be observed from Fig. 7 that the mean Nusselt number $\overline{Nu}$ exhibits a mild increase with increasing Ri before becoming mostly insensitive to the changes in Richardson number Ri for Newtonian fluids (i.e. $Bn = 0$). This behaviour is qualitatively different from the behaviour reported for the C1 configuration (in which the rotating top cover is hotter than the bottom one) by Turan et al. [17]. In the C1 configuration, $\overline{Nu}$ shows a decreasing trend with increasing Ri for Newtonian fluids (i.e. $Bn = 0$) and also for small values of Bing-

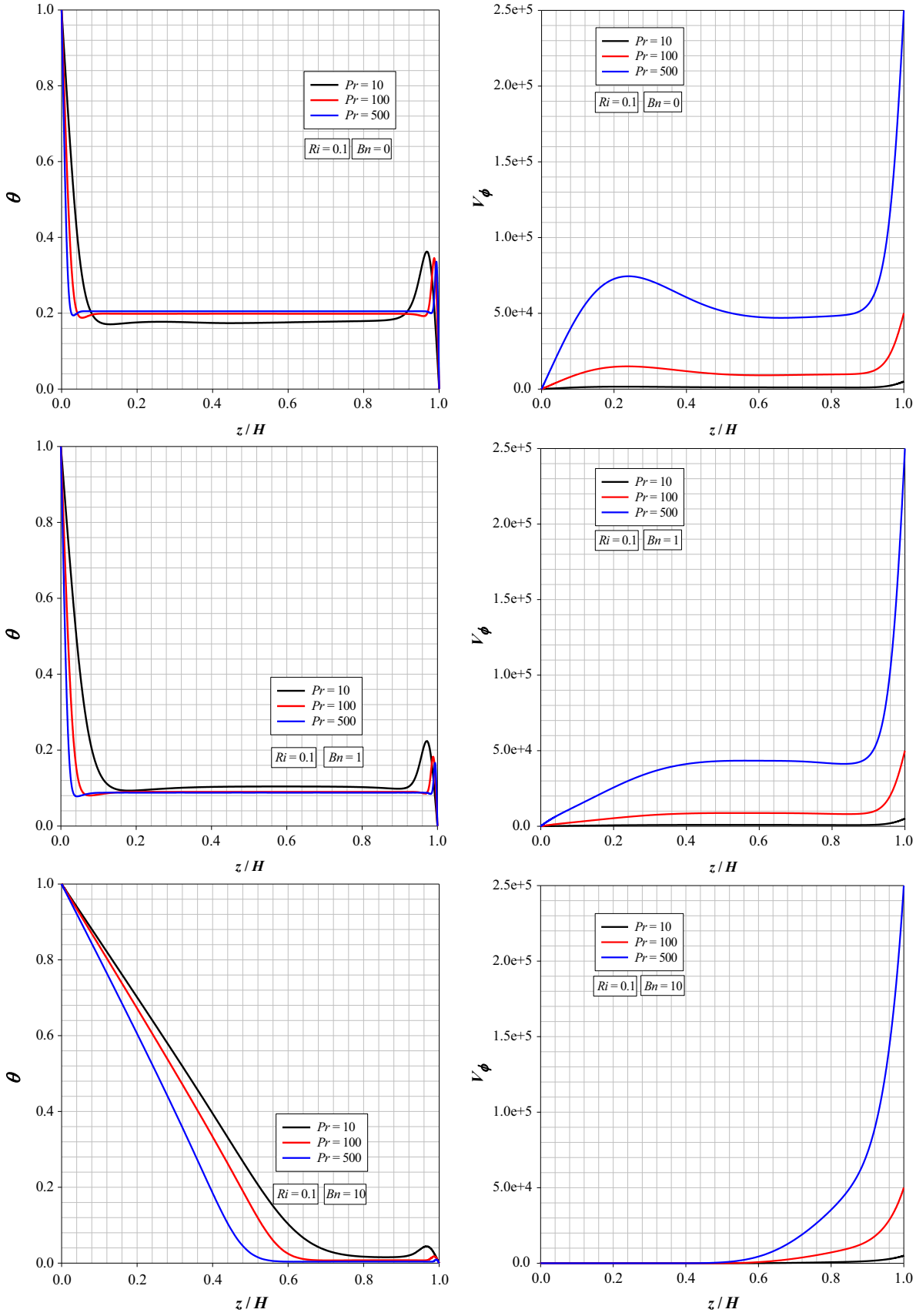

Fig. 11. The variation of non-dimensional temperature θ and swirl velocity component V_ϕ along the vertical mid-plane (i.e. $r/R = 0.5$) for different Pr values for Newtonian (i.e. $Bn = 0$) and Bingham Fluid (i.e. $Bn = 1$ and 10) cases at $Ri = 0.1$ at $Re = 1000$.

Table 3
Summary of the mean Nusselt number $\overline{Nu}$ correlation for Newtonian fluids.

$\overline{Nu} = 1 + k_0 Re^{m_0}$
$10 \leq Pr < 100$
$k_0 = (0.056 + 0.012lnPr) + (0.129lnPr - 0.225)\exp(-Ri(3.368 + 3.123lnPr))$
$m_0 = (0.757 - 0.050nPr) + (0.422lnPr - 0.897)Ri^{(0.118lnPr - 0.083)}$
$100 \leq Pr \leq 500$
$k_0 = (0.207lnPr - 0.605)\exp(-Ri(0.177 + 0.004lnPr))$
$m_0 = (0.683 - 0.008lnPr) + (0.006 + 0.004nPr)Ri^{(0.590 + 0.016lnPr)}$

ham number, whereas $\overline{Nu}$ remains insensitive to the changes in Ri in the case of large Bingham number [17]. This difference in the variation of $\overline{Nu}$ with Ri between the C1 and C2 configurations can be explained in the following manner. For mixed convection (i.e. $Ri > 0$), the relative strengths of inertial, buoyancy and viscous forces determine the flow behaviour. For $Ri = 0$, which corresponds to purely forced convection, the flow is governed by the inertial and viscous forces. The influence of buoyancy force starts to strengthen with an increase in Ri, and therefore the competition between buoyancy force and viscous forces becomes increasingly important with increasing Ri. However, in the C1 configuration, where the top cover is hotter than the bottom one, represents a stable configuration where the lighter hot fluid sits on top of the heavier cold fluid so the effects of natural convection only remain significant close to the heated top cover in the container and oppose the fluid motion induced by top rotating wall. As a result of this, advective transport weakens and the mean Nusselt number decreases with increasing Ri for small values of Bn in the C1 configuration. For large values of Bn, the region of non-negligible value of

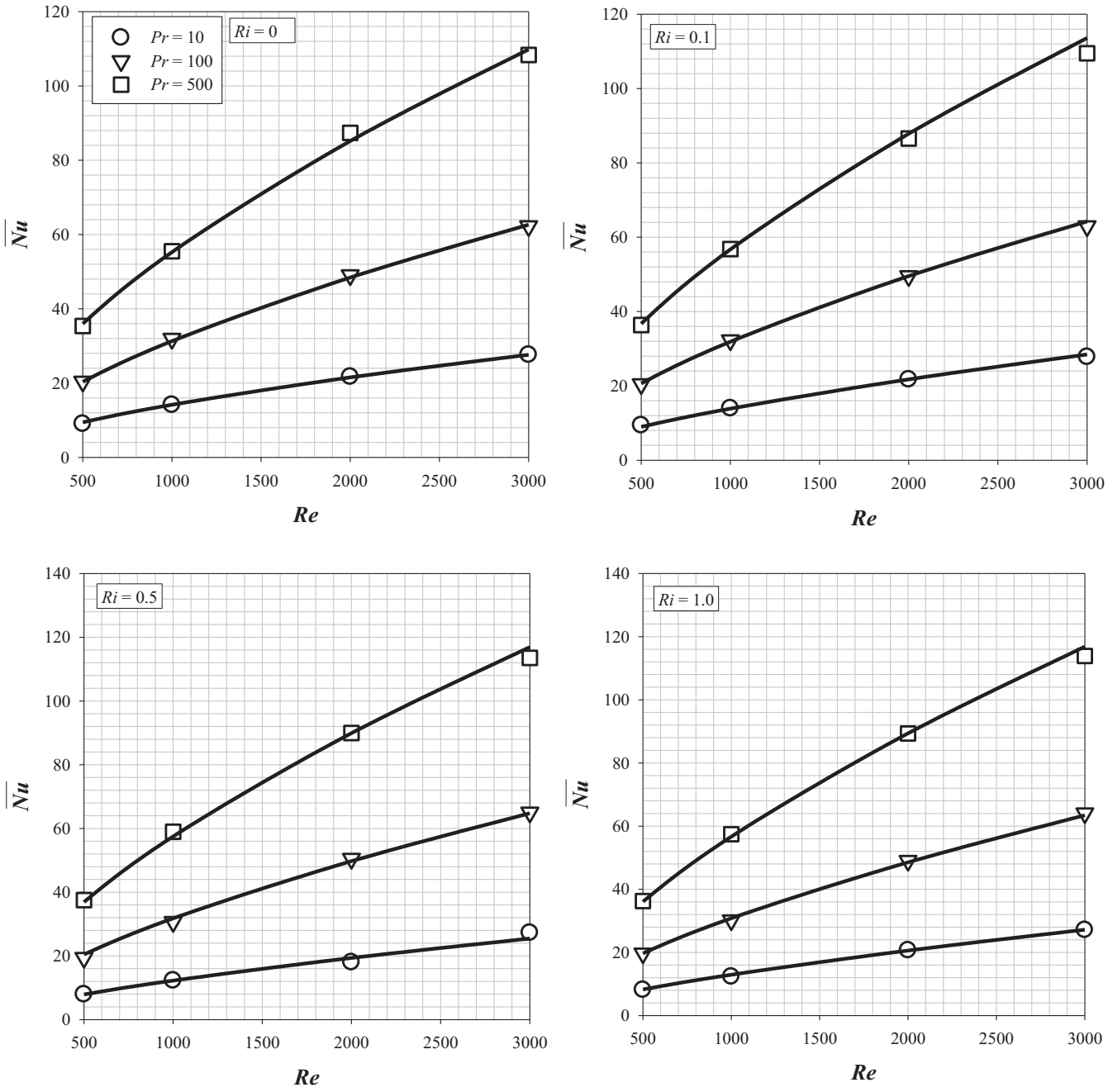

Fig. 12. Comparison between $\overline{Nu}$ obtained from the simulations with the predictions of Eq. (21) for Newtonian fluid cases for different Ri, Re and Pr values.

Table 4
Summary of the mean Nusselt number correlation for Bingham fluids.

$$\overline{Nu} = Max\left[1, \frac{\overline{Nu}_{Bn=0}}{\left(\frac{Bn}{A}+\sqrt{\left(\frac{Bn}{A}\right)^2+1}\right)D}\right]$$

$A = 2\sqrt{aRe + b(RiRe^2)^{1/2}}$ $\rightarrow a = e^{-Ri}$ and $b = 1 - e^{-Ri}$

$D = 1 + k_1 Bn^{m_1}$ $\rightarrow k_1 = a_1\exp(-b_1 Re)$ and $m_1 = a_2 Re^{b2}$

$10 \le Pr \le 100$

$a_1 = (0.139Pr^{0.244}) + (0.772Pr^{0.289-0.568Ri})\exp(0.284Ri)$

$b_1 = (1/(4972.702 + 637.381Pr)) + (1/(1263.822 - 3.710Pr)\exp(-Ri(0.018 + 0.109\ln Pr)$

$a_2 = (1/(0.313 + 1.108Pr)) + (0.139Pr^{0.184+1.333Ri})\exp(-7.968Ri)$

$b_2 = (1 + (5.622 - 0.612lnPr)Ri)/((3.922 + 0.00156lnPr) + (18.263 - 2.627nPr)Ri)$

$100 < Pr \le 500$

$a_1 = (1.559lnPr - 7.369) + (2.404Pr^{0.072-1.909Ri})\exp(3.226Ri)$

$b_1 = (1/(85170 - 161.062Pr)) + (1/(792.7 - 0.153Pr))\exp(-Ri(16.908 - 2.412lnPr))$

$a_2 = 0.00126 + (0.37 - 0.0085lnPr)Pr^{4.359Ri}\exp(-29.215Ri)$

$b_2 = (1 + (287.523 - 4.466lnPr)Ri)/((6.037 - 0.423lnPr) + (21.879 - 3.821lnPr)Ri)$

V_ϕ remains confined to the vicinity of the rotating top cover in the C1 configuration and thus the strength of advective transport and the mean Nusselt number $\overline{Nu}$ are not significantly affected by the variation of Ri. By contrast, in the C2 configuration, where the rotating top cover is colder than the bottom one, the buoyancy force strengthens with increasing Ri and this buoyancy-induced flow aids the fluid motion initiated by the rotating end cover for small values of Ri and this leads to a marginal increase in the mean Nusselt number $\overline{Nu}$. A comparison of the distributions of V_ϕ for different values of Ri in Fig. 8 reveals that the velocity magnitude increases with increasing Ri in comparison to the pure forced convection (i.e. $Ri = 0$) case. However, the hydrodynamic boundary layer thicknesses on both top and bottom covers do not change appreciably with a change in Ri for large values of Richardson number (see Fig. 8), and the same is applicable for the thermal boundary layer. Thus, the mean Nusselt number $\overline{Nu}$ either does not change appreciably or decrease slightly with increasing Richardson number for large values of Ri. This Richardson number dependence of the mean Nusselt number becomes increasingly weak for an increase in Bingham number, which is consistent with the Nusselt number scaling presented in Table 2. The Richardson number dependence of the mean Nusselt number can alternatively explained in terms of an effective Grashof number for Bingham fluid flows in the following manner:

$$Gr_{eff} = \frac{\rho^2 g\beta\Delta T R^3}{\mu_{eff}^2} = \frac{Gr(a + bRi^{1/2})^2}{\left[(a + bRi^{1/2}) + \left(\frac{Bn^2}{2Re} + \frac{Bn}{2Re}\sqrt{Bn^2 + 4[aRe + bReRi^{1/2}]}\right)\right]^2} \quad (20)$$

Eqs. (19) and (20) suggest that both the effective Grashof number Gr_{eff} and the effective Reynolds number Re_{eff} increase with increasing Ri for mixed convection cases. This indicates that the relative influences of both buoyancy and inertial forces strengthen in comparison to viscous forces with increasing Ri. This leads to an increase in the mean Nusselt number $\overline{Nu}$ with Ri as observed in Fig. 7. However, the mean Nusselt number eventually becomes a weak decreasing function of Ri for large values of Richardson number according to the scaling estimate of $\overline{Nu}$ given in Table 2. Moreover, the increases of effective Grashof and Reynolds numbers with an increase in Ri weaken with increasing Bn. Therefore, the relative influences of the buoyancy and inertial forces in comparison to viscous forces weaken for large values of Bn. As a result of this, the mean Nusselt number $\overline{Nu}$ becomes insensitive to the changes in Ri for large values of Bn, as observed in Fig. 7.

It can indeed be seen from Fig. 8 that the distributions of non-dimensional swirling velocity component V_ϕ is affected by Ri for small values of Bn, whereas Ri does not have any influence on the non-dimensional swirl velocity component V_ϕ for large values of Bingham number Bn. This suggests that the convection strength and thereby the mean Nusselt number $\overline{Nu}$ become insensitive to the variation of Richardson number Ri for large values of Bn, as shown in Fig. 7. In addition, it can be seen from Fig. 7 that there is a step change in the numerical value of $\overline{Nu}$ at $Ri = 0.3$ for $Bn = 1.0$. In order to ascertain whether this step change arises due to a physical realisable mechanism, some additional simulations have been carried out using more refined meshes for the same set of Bn, Re, and Ri values. It was observed that the same trend also appears for the other meshes. This indicates that this step change in the numerical value of $\overline{Nu}$ is a physical reality. It can be seen from the contours of non-dimensional stream functions in Fig. 9 that the flow pattern changes at $Ri = 0.3$ where a step change in the value of $\overline{Nu}$ occurs. A second cellular structure appears on the bottom cover (i.e. hot cover) at $Ri = 0.3$, whereas only one cell flow structure is observed for smaller values of Richardson number. The second cell grows gradually with increasing Ri for $Bn = 1$ at $Re = 1000$ and $Pr = 100$. Eqs. (19) and (20) indicate that the effective values of Reynolds and Grashof numbers change with the variation of Ri and thus a flow structure, which can be realised for small values of Ri, may not be possible to obtain for large values of Ri.

3.4. Variations of Prandtl number

The variations of $\overline{Nu}$ with Pr for Newtonian ($Bn = 0$) and Bingham fluids ($Bn = 1$ and 10) for both $Ri = 0$ (pure forced convection) and $Ri = 0.1$ (mixed convection) cases are shown in Fig. 10, which indicates that $\overline{Nu}$ increases with increasing Pr for the C2 configuration, which is qualitatively similar to the results reported by Turan et al. [17] for the C1 configuration. In addition to this, it can be detected from Fig. 10 that Pr has significant influences on $\overline{Nu}$ for small values of Bn for both $Ri = 0$ and 0.1 cases, whereas $\overline{Nu}$

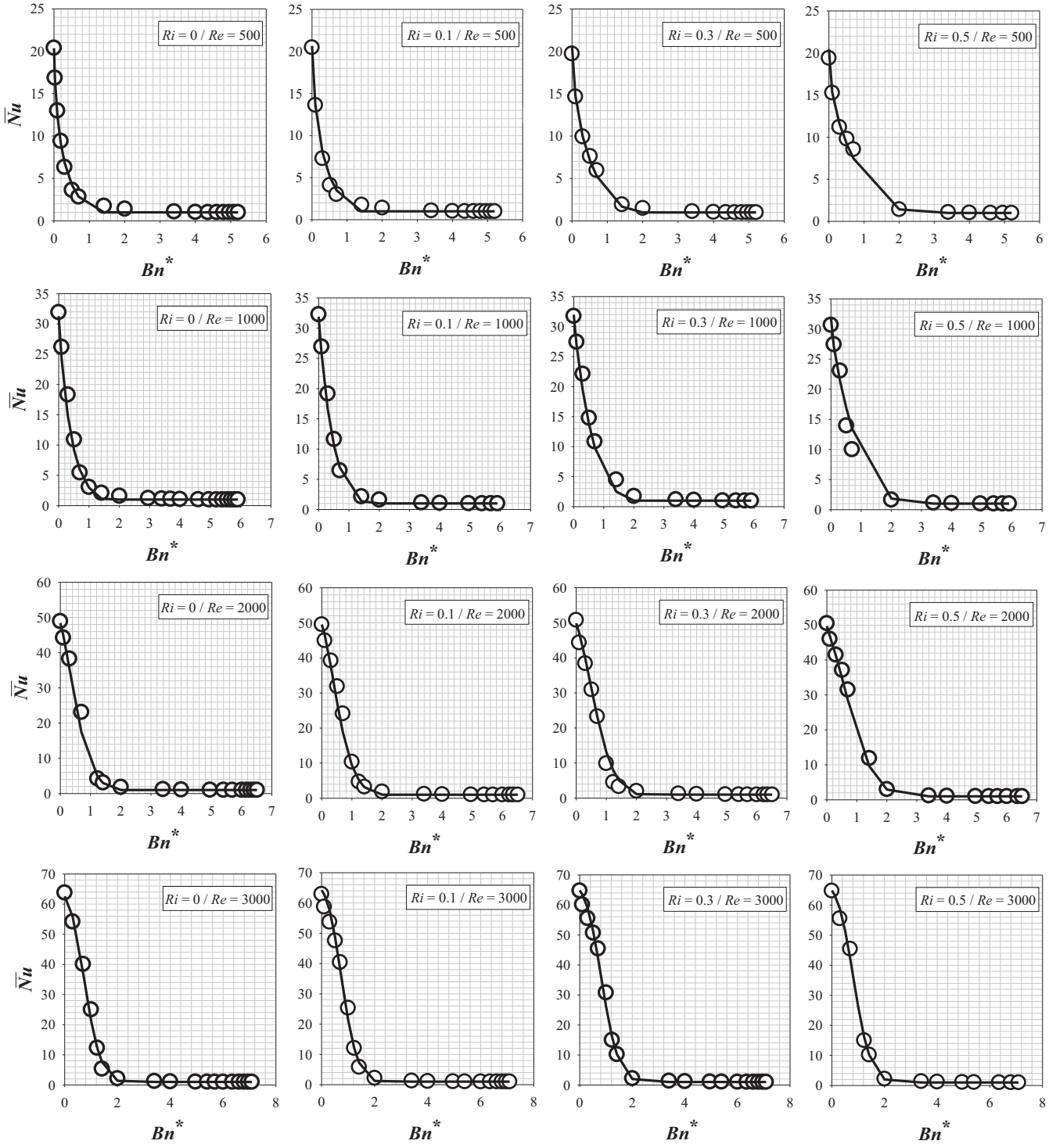

Fig. 13. Comparison between $\overline{Nu}$ obtained from the simulations with the predictions of Eq. (22) for Bingham fluid cases for different *Ri* and *Re* values at *Pr* = 100.

becomes insensitive to the variation of *Pr*. for large values of *Bn*. This behaviour can be explained by the distributions of θ and V_ϕ along the vertical mid-plane which are shown in Fig. 11 for $Ri = 0.1$. It is apparent from Fig. 11 that the thermal boundary layer thickness decreases with increasing *Pr* for small values of Bingham number, which in turn acts to increase the mean Nusselt number $\overline{Nu} \sim R/\delta_{th}$. Furthermore, the magnitude of the non-dimensional swirling velocity component rises with increasing *Pr* for all Bingham fluid cases. This indicates that the advective transport strengthens with increasing *Pr*, which is consistent with previous findings [8]. This behaviour is observed all along the vertical mid-plane for small values of *Bn*, whereas it appears only in the vicinity of the heated bottom cover for large *Bn* values. Therefore, $\overline{Nu}$ is less sensitive to the variation of *Pr* for large values of *Bn* as shown in Fig. 10.

The strengthening of advection with increasing *Pr* can also be explained with the help of Eq. (15a), which indicates that advective transport within the boundary layer strengthens with increasing *Pr* especially for small *Bn* values. This leads to an increase in $\overline{Nu}$ with increasing *Pr* as observed in Fig. 10. However, Eq. (15a) also shows

that this strengthening of advection with increasing *Pr* decreases with increasing *Bn* values since advective transport weakens with increasing *Bn*. As a result, $\overline{Nu}$ becomes less sensitive to the variation of *Pr* for large values of *Bn*.

3.5. The mean Nusselt number correlation

According to the Buckingham's pi theorem it is possible to show that the mean Nusselt number $\overline{Nu}$ can be expressed as: $\overline{Nu} = f_1(Bn,\ Re,\ Ri,\ Pr)$. In addition to this, the scaling analysis indicates the same qualitative trend for the mean Nusselt number in this configuration. In the case of Newtonian fluids (i.e. $Bn = 0$), the following correlation is proposed for the mean Nusselt number $\overline{Nu}$ for $0 \le Ri \le 1$, $500 \le Re \le 3000$ and $10 \le Pr \le 500$:

$$\overline{Nu}_{Bn=0} = 1 + k_0 Re^{m_0} \tag{21}$$

where k_o and m_o are the correlation parameters which depend on *Ri* and *Pr* (Table 3). These parameterisations of the *Ri* and *Pr* dependences of k_o and m_o are empirical in nature but they ensure that Eq. (21) is consistent with the Buckingham's pi theorem (i.e. $\overline{Nu} = f_2(Re, Ri, Pr)$). The predictions of the correlation given by Eq. (21) are compared to the numerical results in Fig. 12 for different *Ri*, *Re* and *Pr* values. Fig. 12 demonstrates that the correlation, given by Eq. (21), satisfactorily captures both qualitative and quantitative variations of $\overline{Nu}$ for the range of *Ri*, *Re* and *Pr* analysed in this study.

In addition, based on the scaling relation given in Table 2, a correlation for the mean Nusselt number for Bingham fluids is also proposed here for $0 \le Ri \le 1$, $500 \le Re \le 3000$ and $10 \le Pr \le 500$:

$$\overline{Nu} = Max\left[1, \frac{\overline{Nu}_{Bn=0}}{\left(\frac{Bn}{A} + \sqrt{\left(\frac{Bn}{A}\right)^2 + 1}\right)D}\right] \tag{22}$$

where $A = 2\sqrt{aRe + b(RiRe^2)^{1/2}}$ with $a = e^{-Ri}$ and $b = 1 - e^{-Ri}$. Here, D is empirically expressed as: $D = 1 + k_1 Bn^{m_1}$ where k_1 and m_1 are the correlation parameters, which are listed in Table 4. For $= 0$, Eq. (22) reduces to the mean Nusselt number correlation for Newtonian fluids (i.e. Eq. (21)). By contrast, for $Bn \geqslant Bn_{max}$, the mean Nusselt number $\overline{Nu}$ approaches unity due to conduction-driven transport. The predictions of Eq. (22) are compared to the numerical data in Fig. 13 for different *Ri*, *Re* at *Pr* = 100, which demonstrates that the correlation given by Eq. (22) satisfactorily captures the qualitative variations of $\overline{Nu}$ with *Bn* for the range of *Ri*, *Re* at *Pr* = 100. The correlation function given by Eq. (22) can approximately estimate the numerical results at the level of an average error of 8%. It is also worth noting that the same level of quantitative agreement between numerical results and the correlation given by Eq. (22) has also been obtained for *Pr* = 10 and 500 values analysed in this study.

4. Conclusions

The influences of Bingham, Reynolds, Prandtl, and Richardson numbers on the mean Nusselt number for steady-state laminar mixed convection of yield stress fluids obeying the Bingham model in cylindrical enclosures with a rotating top cover have been numerically analysed for the configuration where the bottom cover is kept at a higher temperature than the rotating top cover (i.e. C2 configuration). It has been found that the qualitative nature of the Bingham, Reynolds and Prandtl number dependences of the mean Nusselt number are the same as in the configuration where the top rotating wall is heated (i.e. C1 configuration) [17], whereas the Richardson number dependence of the mean Nusselt number is qualitatively different from the C1 configuration. The mean Nusselt number $\overline{Nu}$ has been found to decrease with an increase in *Bn*, and $\overline{Nu}$ ultimately attains a value of unity, which is indicative of a conduction-driven transport. The mean Nusselt number $\overline{Nu}$ has also been found to increase with increasing Reynolds number due to the strengthening of advective transport. The mean Nusselt number $\overline{Nu}$ exhibits a non-monotonic trend (i.e. increases with increasing *Ri* for small values of Richardson number before showing a weak decreasing trend) with increasing *Ri* for Newtonian fluid (i.e. $Bn = 0$), whereas $\overline{Nu}$ increases with increasing *Ri* for small values of Richardson number before becoming a weak function of *Ri* for Bingham fluids. A step change in the mean Nusselt number has also been observed with an increase in Richardson number for some Bingham number values due to a change in flow pattern. Moreover, both Reynolds number and Richardson number dependences of the mean Nusselt number have been found to weaken considerably with an increase in Bingham number. Detailed physical explanations have been provided for the influences of Bingham, Reynolds, Prandtl, and Richardson numbers on the mean Nusselt number with the help of a scaling analysis. Finally, the scaling results and numerical findings have been utilised to propose a correlation for the mean Nusselt number, which has been shown to capture the simulation data accurately for the parameter range considered here.

Acknowledgements

This study was supported by Newton Research Collaboration Programme and is hereby gratefully acknowledged.

References

[1] H.U. Vogel, Experimentelle Ergebnisse über die laminare Strömung in einem zylindrischen Gahause mit darin rotieren-der Scheibe, MPI Bericht 6, 1968.
[2] H.U. Vogel, Rückströmungsblasen in Drallsströmungen. Festschrift 50 Jahre Max-Planck-Institut für Strömungsforschung 1925–1975, 1975.
[3] B. Ronnenberg, Ein selbstjustierendes 3-Komponenten-Laserdoppler-anemometer nach dem Vergleichsstrahlverfahren, angewandt für Untersuchungen in einer stationaren sylinder-symmetrischen Drehströmung mit einem Rückstromgebiet, MPI Bericht 20, 1977.
[4] M. Bertela, F. Gori, Laminer flow in a cylindrical container with a rotating cover, J. Fluids Eng. 104 (1982) 31–39.
[5] M.P. Escudier, Observations of the flow produced in a cylindrical container by rotating endwall, Exp. Fluids 2 (1984) 189–196.
[6] H.J. Lugt, H.J. Haussling, Axisymmetric vortex breakdown in rotating fluid within a container, Trans. ASME J. Appl. Mech. 49 (1982) 921–923.
[7] J.M. Lopez, Axisymmetric vortex breakdown: Part1. Confined swirling flow, J. Fluid Mech. 221 (1990) 533–552.
[8] C.H. Lee, J.M. Hyun, Flow of a stratified fluid in a cylinder with a rotating lid, Int. J. Heat Fluid Flow 20 (1999) 26–33.
[9] R. Iwatsu, Flow pattern and heat transfer of swirling flows in cylindrical container with rotating top and stable temperature gradient, Int. J. Heat Mass Transfer 47 (2004) 2755–2767.
[10] M.P. Escudier, L.M. Cullen, Flow of a shear-thinning liquid in a cylindrical container with a rotating end wall, Exp. Therm. Fluid Sci. 12 (1996) 381–387.
[11] J.R. Stokes, D.V. Boger, Mixing of viscous polymer liquids, Phys. Fluids 12 (6) (2000) 1411–1416.
[12] B. Traore, C. Castelain, T. Burghelea, Efficient heat transfer in a regime of elastic turbulence, J. Non-Newtonian Fluid Mech. 223 (2015) 62–76.
[13] G. Böhme, L. Rubart, M. Stenger, Vortex breakdown in shear-thinning liquids: experiment and numerical simulations, J. Non-Newtonian Fluid Mech. 45 (1992) 1–20.
[14] A.A. Rashaida, D.J. Bergstrom, R.J. Sumner, Mass transfer from a rotating disk to a Bingham fluid, Trans. ASME J. Appl. Mech. 73 (2006) 108–111.
[15] A. Ahmadpour, K. Sadeghy, Swirling flow of Bingham fluids above a rotating disk: an exact solution, J. Non-Newtonian Fluid Mech. 197 (2013) 41–47.
[16] A. Guha, S. Sengupta, Analysis of von Kármán's swirling flow on a rotating disc in Bingham fluids, Phys. Fluids 28 (2016) 013601.
[17] O. Turan, S. Yigit, N. Chakraborty, Numerical investigation of mixed convection of Bingham fluids in cylindrical enclosures with heated rotating top wall, Int. J. Heat Mass Transfer 108 (2017) 1850–1869.
[18] M. Darbouli, C. Metivier, J.M. Piau, A. Magnin, A. Abdelali, Rayleigh-Benard convection for viscoplastic fluids, Phys Fluids 25 (2013) 023101.
[19] Z. Kebiche, C. Castelain, T. Burghelea, Experimental investigation of the Rayleigh- Benard convection in a yield stress fluid, J. Non-Newtonian Fluid Mech. 203 (2014) 9–23.

[20] H.A. Barnes, The yield stress—a review or '$\pi\alpha\nu\tau\alpha\rho\varepsilon\iota$'—everything flows?, J Non-Newt. Fluid Mech. 81 (1999) 133–178.
[21] E.J. O'Donovan, R.I. Tanner, Numerical study of the Bingham squeeze film problem, J. Non-Newtonian Fluid Mech. 15 (1984) 75–83.
[22] J. Peixinho, C. Desaubry, M. Lebouche, Heat transfer of a non-Newtonian fluid (Carbopol aqueous solution) in transitional pipe flow, Int. J. Heat Mass Transfer 51 (2008) 198–209.
[23] R.J. Poole, R.P. Chhabra, Development length requirements for fully-developed laminar pipe flow of yield stress fluids, ASME J. Fluids Eng. 132 (3) (2010) 034501.
[24] M.P. Escuider, J. O'Leary, R.J. Poole, Flow produced in a conical container by a rotating end wall, Int. J. Heat Fluid Flow 28 (2007) 1418–1428.
[25] S.V. Patankar, Numerical Heat Transfer and Fluid Flow, Hemisphere, Washington, D.C., 1980.
[26] O. Turan, N. Chakraborty, R.J. Poole, Laminar natural convection of Bingham fluids in a square enclosure with differentially heated side walls, J. Non-Newtonian Fluid Mech. 165 (2010) 901–913.
[27] E. Mitsoulis, T. Zisis, Flow of Bingham plastics in a lid-driven square cavity, J. Non-Newtonian Fluid Mech. 101 (2001) 173–180.